Journal of Statistical Physics, Vol. 101, Nos. 1/2, 2000

The Nosé–Hoover Thermostated Lorentz Gas

K. Rateitschak,[1] R. Klages,[1] and Wm. G. Hoover[2]

Received November 22, 1999; final July 14, 2000

We apply the Nosé–Hoover thermostat and three variations of it, which control different combinations of velocity moments, to the periodic Lorentz gas. Switching on an external electric field leads to nonequilibrium steady states for the four models. By performing computer simulations we study the probability density, the conductivity and the attractor in nonequilibrium. The results are compared to the Gaussian thermostated Lorentz gas and to the Lorentz gas as thermostated by deterministic scattering. We find that slight modifications of the Nosé–Hoover thermostat lead to different dynamical properties of our models. However, in all cases the attractor appears to be multifractal.

KEY WORDS: Nonequilibrium steady states; chaotic transport; Nosé–Hoover thermostat; multifractal attractor; periodic Lorentz gas.

1. INTRODUCTION

In a system of particles under an external force a nonequilibrium steady state can be obtained by applying a thermostat.[1–3] Deterministic and time-reversible bulk thermostating is based on introducing a momentum-dependent friction coefficient in the equations of motion. One such mechanism is the Nosé–Hoover thermostat.[4, 5] It creates a canonical ensemble in equilibrium and yields a stationary distribution of velocities in nonequilibrium. Another version, the Gaussian isokinetic thermostat,[6–8] leads to a microcanonical density for the velocity components in equilibrium and to a constant kinetic energy in nonequilibrium. Though the microscopic dynamics of these thermostated systems is time-reversible the

[1] Center for Nonlinear Phenomena and Complex Systems, Université Libre de Bruxelles, Campus Plaine CP 231, Blvd du Triomphe, B-1050 Brussels, Belgium. E-mail: krateits@ulb.ac.be

[2] Department of Applied Science, University of California at Davis/Livermore, and Methods Development Group, Lawrence Livermore National Laboratory, Livermore, California 94551-7808.

0022-4715/00/1000-0061$18.00/0

macroscopic dynamics is irreversible in nonequilibrium.[9] This is related to a contraction onto a fractal attractor characterized by a Lyapunov spectrum with a negative sum.[10–13]

The comparison of different thermostating mechanisms and the identification of their common properties is crucial to obtain a general characterization of nonequilibrium steady states.[14–16] Standard bulk thermostating schemes like Gauss and Nosé–Hoover have led to the conclusion that nonequilibrium steady states generated by time-reversible thermostats are characterized by the existence of fractal attractors. These attractors, in turn, furnish an identity between irreversible entropy production and phase-space contraction.[9, 16–19] Moreover, this identity is at the heart of specific formulas relating transport coefficients to Lyapunov exponents.[10, 17, 20] We remark that the physicality of this thermostated systems approach to nonequilibrium has been questioned in refs. 14, 15, and 21.

The characteristic features of thermostated many-particle systems have been recovered for a specific one-particle system, the Gaussian thermostated Lorentz gas.[10, 11, 18, 19, 22–25] The periodic Lorentz gas consists of a particle that moves through a triangular lattice of hard disks and is elastically reflected at each disk collision.[3] It serves as a standard model in the field of chaos and transport, see refs. 13–15. A one-particle system reflects more strongly and transparently the nonequilibrium properties induced by a thermostat. For this reason the Lorentz gas is an appropriate tool to compare the properties of nonequilibrium steady states obtained from different deterministic and time-reversible thermostating mechanisms.

We perform such a comparison by applying the Nosé–Hoover thermostat and some variations of it to the periodic Lorentz gas. However, we also want to consider an alternative thermostating mechanism, thermostating by deterministic scattering, which has recently been introduced for the periodic Lorentz gas.[27, 28] [4] This deterministic and time-reversible mechanism is based on including energy transfer between the moving particle and the disk scatterer at the moment of collision, rather than using a momentum-dependent friction coefficient. It leads to a canonical probability density for the particle in equilibrium, and in nonequilibrium it keeps the energy of the particle on average constant. Thus, the method of thermostating by deterministic scattering is closer to the Nosé–Hoover thermostat then to the Gaussian thermostat.

[3] A model almost identical to the driven periodic Lorentz gas, except for some geometric restrictions, is the Galton board, which was invented in 1873 to study probability distributions.[26]

[4] This mechanism was applied later to a system of hard disks under a temperature gradient and shear.[29]

Our goal is to study numerically the probability density, the conductivity and the attractor in nonequilibrium. Furthermore, it is known that for the Gaussian thermostated Lorentz gas a complicated dependence of the attractor on the field strength results,[10, 22, 23] which we also study for the different thermostats. In addition, we briefly elaborate on the identity between phase-space contraction and entropy production. We then ask which common properties the Nosé–Hoover thermostat and its variations share with the Gaussian thermostat and with thermostating by deterministic scattering, and which properties depend on the specific choice of the thermostat. In Section 2 we introduce the Nosé–Hoover thermostat and discuss some variations of it. In Section 3 we define the periodic Lorentz gas and the thermostats we study. We investigate these models in equilibrium in Section 4 and in nonequilibrium in Section 5. Conclusions are drawn in Section 6.

2. THE NOSÉ–HOOVER THERMOSTAT AND SOME VARIATIONS

In the following sections we consider a one-particle system in two dimensions with the position coordinates $\vec{q} = (q_x, q_y)$ and the momentum coordinates $\vec{p} = (p_x, p_y)$. The mass of the particle is set equal to unity. The equations of motion for the Nosé–Hoover thermostated particle are then given by[5]

$$\begin{aligned} \dot{\vec{q}} &= \vec{p} \\ \dot{\vec{p}} &= \vec{\varepsilon} - \zeta \vec{p} \\ \dot{\zeta} &= \left(\frac{p^2}{2T} - 1 \right) \frac{1}{\tau^2} \end{aligned} \tag{1}$$

The thermostat variable ζ couples the particle dynamics to a reservoir. It controls the kinetic energy of the particle $p^2/2$ such that $\langle p^2 \rangle = 2T$. This relation holds even in nonequilibrium as induced by an electric field $\vec{\varepsilon}$. τ is the response time of the thermostat. Taking the limit $\tau \to 0$ in Eqs. (1) results in the Gaussian thermostat with $\zeta = (\vec{\varepsilon} \cdot \vec{p})/p^2$. In the limit $\tau \to \infty$ the friction coefficient approaches a constant, $\zeta = \zeta_c$, and the equations of motion are not time-reversible anymore. The dynamics of this dissipative limit has been investigated in ref. 30.

A generalization of the Nosé–Hoover thermostat to control higher even moments of p was introduced by Hoover.[31] The moments are fixed according to the momentum relations for the Gaussian distribution. This

more detailed control of the nonequilibrium steady state can improve statistical dynamical properties, like ergodicity, as has been shown for the Nosé–Hoover thermostated harmonic oscillator.[32, 33] In principle the method of the control of the even moments can straightforwardly be extended to the control of the odd moments. The control of the odd moments involves a thermostat variable for the particle *current*. That means the conductivity is an additional parameter beside the temperature. This is physically undesirable, apart from the fact that the respective equations of motion would not be time-reversible anymore.

We briefly note that there exist other formal generalizations,[34] or modifications,[35, 36] of the Nose-Hoover thermostat in the literature. They have been critically reviewed in refs. 31–33.

3. VARIATIONS OF THE NOSÉ–HOOVER THERMOSTAT FOR THE PERIODIC LORENTZ GAS

The basic thermostating method we investigate in this paper is the Nosé–Hoover thermostat, Eqs. (1). The structure of the equations of motion allows to construct infinitely many variations without destroying the basic properties of time reversibility and by keeping the kinetic energy on average constant such that $\langle p^2 \rangle = 2T$. In the following we introduce three specific variations of it, as we argue below:

The *first variation* is the Nosé–Hoover thermostat with a field dependent coupling to the reservoir,

$$\begin{aligned} \dot{\vec{q}} &= \vec{p} \\ \dot{p}_x &= \varepsilon_x - (1+\varepsilon_x)\,\zeta p_x \\ \dot{p}_y &= -\zeta p_y \\ \dot{\zeta} &= \left(\frac{p^2}{2T} - 1\right)\frac{1}{\tau^2} \end{aligned} \tag{2}$$

which is obtained by including the factor $1+\varepsilon_x$ in Eqs. (1). Here the coordinate system is chosen such that the field direction is parallel to the x-axis. The strength of the coupling between particle and reservoir is thus adjusted to the anisotropy induced by the field. The standard Nosé–Hoover thermostat Eqs. (1) is contained as a special case in equilibrium. Alternatively, these equations can be written by defining two field-dependent friction coefficients, $\xi_x = (1+\varepsilon_x)\,\zeta$ and $\xi_y \equiv \zeta$, which are governed by $\dot{\xi}_x = (p^2/2T - 1)(1+\varepsilon_x)/\tau^2$ and $\dot{\xi}_y = (p^2/2T - 1)/\tau^2$, respectively. It then becomes clear that for each momentum component there exists a separate reservoir

response time. These are $\tau/\sqrt{1+\varepsilon_x}$ and τ. With increasing field strength the corresponding response time decreases.

The *second variation* first introduced in ref. 31 includes control of $\langle p^4 \rangle = 8T^2$,

$$\begin{aligned}
\dot{\vec{q}} &= \vec{p} \\
\dot{\vec{p}} &= \vec{\varepsilon} - \zeta_1 \vec{p} - \zeta_2 \frac{p^2}{2T} \vec{p} \\
\dot{\zeta}_1 &= \left(\frac{p^2}{2T} - 1 \right) \frac{1}{\tau^2} \\
\dot{\zeta}_2 &= \frac{p^2}{2T} \left(\frac{p^2}{2T} - 2 \right) \frac{1}{\tau^2}
\end{aligned} \tag{3}$$

As described in the previous sections this variation can improve statistical dynamical properties, like ergodicity.

The *third variation* controls p_x^2 and p_y^2 separately. This is performed by defining two independent reservoirs for the x and y directions,

$$\begin{aligned}
\dot{\vec{q}} &= \vec{p} \\
\dot{p}_x &= \varepsilon_x - \zeta_x p_x \\
\dot{p}_y &= \varepsilon_y - \zeta_y p_y \\
\dot{\zeta}_x &= \left(\frac{p_x^2}{T} - 1 \right) \frac{1}{\tau_x^2} \\
\dot{\zeta}_y &= \left(\frac{p_y^2}{T} - 1 \right) \frac{1}{\tau_y^2}
\end{aligned} \tag{4}$$

This variation intervenes more deeply in the microscopic dynamics by forcing the single components p_x^2 and p_y^2 separately towards canonical distributions. However, in contrast to the previous variations a curiosity is hidden in it: At every collision the thermostat variables ζ_x and ζ_y are uncorrelated to the thermostated variables p_x and p_y, because p_x and p_y change at a collision whereas ζ_x and ζ_y remain the same. Therefore the thermostat does not work efficiently. But we have not found any reflection of this curiosity in the macroscopic behavior.

In exactly the same way as the Nosé–Hoover thermostat[37] the third variation with the separate control of p_x^2 and p_y^2 can be derived from a Hamiltonian. One can argue that the first variation is a special case of the

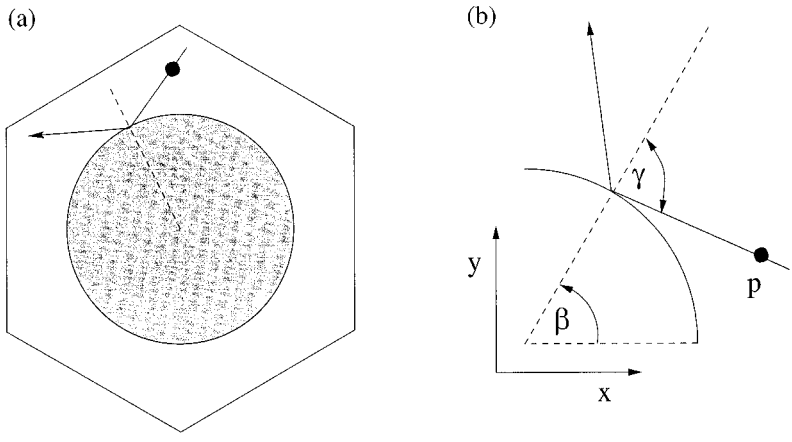

Fig. 1. (a) Elementary cell of the periodic Lorentz gas on a triangular lattice, and (b) the relevant variables.

Nosé–Hoover thermostat, which allows us to draw conclusions about the existence of a Hamiltonian for it, as is discussed in detail in ref. 38. Perhaps the second variation can likewise be derived from a Hamiltonian. Although this variation has already been used extensively in the literature[32, 33] no equivalent Hamiltonian has been given.

We study the dynamics of these models for the Lorentz gas cell with periodic boundaries, as indicated in Fig. 1a. As the radius of the disk we take $r = 1$. For the spacing between two neighboring disks we choose $w \simeq 0.2361$, corresponding to a density equal to 4/5 of the maximum packing density of the scatterers. A collisionless free flight of the particle is avoided for this parameter.[10] The relevant variables of the dynamical system are depicted in Fig. 1b: β is the angular coordinate of the point at which the particle elastically collides with the disk, and γ is the angle of incidence at this point. Unless declared otherwise the temperature is chosen to $T = 0.5$.

Between collisions, the equations of motion are integrated by a fourth-order Runge–Kutta algorithm with a step size of $dt = 0.005$.[24] Whenever a collision occurs, the collision of the particle with the disk has been determined with a precision of 10^{-7}.[5]

[5] We have checked our program by applying it to the Gaussian thermostated Lorentz gas. The qualitative (attractor) and quantitative results (conductivity) agree with the results in ref. 23. We have also verified our results for the Nosé–Hoover thermostat and for the three variations by doing some test runs with a step size of $dt = 0.0001$. The dependence of the results on the step size was insignificant.

4. EQUILIBRIUM

For equilibrium systems with mixing dynamics, Nosé–Hoover type thermostats should generate a canonical probability density as the stationary solution of the Liouville equation. However, as is discussed in the following, only the third variation yields a canonical distribution in equilibrium, that is, only this variation appears to be mixing.

Inserting the initial condition $(p_0, \zeta_0) = (\sqrt{2T}, 0)$ in Eqs. (1) with $\varepsilon = 0$ the velocity of the particle becomes a constant, $p = \sqrt{2T}$, that means the Nosé–Hoover thermostat does not act in the Lorentz gas and the dynamics is microcanonical. For other initial conditions one observes in computer simulations that p^2 and ζ oscillate periodically and that the dynamics of this one-particle system is nonergodic.

A stability analysis confirms the numerical results: The Nosé–Hoover thermostated equations of motion Eqs. (1) can be reduced for $\varepsilon = 0$ to

$$\begin{aligned} \dot{p^2} &= -2\zeta p^2 \\ \dot{\zeta} &= \left(\frac{p^2}{2T} - 1\right)\frac{1}{\tau^2} \end{aligned} \tag{5}$$

Eqs. (5) are also valid at the moment of a collision, because p^2 and ζ are not changed by a collision. The fixed point of Eqs. (5) is $(p^2, \zeta) = (2T, 0)$ with the eigenvalues $\lambda_{1/2} = \pm\sqrt{-4T/\tau^2}$ and is thus elliptic.

The additional control of $\langle p^4 \rangle$, see Eq. (4), destroys the microcanonical probability density but it is not sufficient to obtain a mixing dynamics in the periodic Lorentz gas. Different initial conditions still lead to a different shape of the momentum probability density $\varrho(p_x)$. In contrast, the separate control of p_x^2 and p_y^2 leads to a mixing dynamics in equilibrium corresponding to the canonical probability density $\varrho(p_x)$.[39]

5. NONEQUILIBRIUM

We now apply an external electric field $\vec{\varepsilon}$ parallel to the x-axis. The Nosé–Hoover thermostat and the related models then lead to well defined nonequilibrium steady states with constant average energy of the particle.

The precise definition of temperature in nonequilibrium is problematic,[3] but the discussions in refs. 2 and 13 provide a kinetic-theory argument supporting the usual choice. We follow here the argument of ref. 29: In equilibrium the temperature of the particle and of the thermal reservoir is unambiguously defined by $T = \langle v^2 \rangle/2$. In nonequilibrium the temperature

of the particle is defined by the kinetic energy in the comoving frame, $T_K = (\langle v^2 \rangle - \langle v_x \rangle^2)/2$. However, the kinetic energy in the fixed frame T is still relevant for tuning the interaction between particle and reservoir, such that T can be defined as the reservoir temperature. This is the notation conventionally used in the literature,[3] which we apply here as well.

5.1. Probability Density $\varrho(p_x)$

In this subsection we have chosen $T = 0.60029$ which corresponds to the reservoir temperature we found in a system thermostated by deterministic scattering at a parametric temperature of $T = 0.5$ and at a field strength of $\varepsilon = 0.5$.[27, 28]

The momentum probability density $\varrho(p_x)$ for the Nosé–Hoover thermostat for $\varepsilon = 0.5$ is presented in Fig. 2a. For $\tau^2 = 0.01$ the density shows some similarity to the deformed microcanonical density of the Gaussian thermostat appearing in the limit $\tau \to 0$, whereas for $\tau^2 = 1$ and $\tau^2 = 1000$ the density becomes similar to the density of thermostating by deterministic scattering, which is related to a canonical distribution.[27, 28]

Figure 2b shows $\varrho(p_x)$ for the three variations of the Nosé–Hoover thermostat. The density of the Nosé–Hoover thermostat with field-dependent coupling to the reservoir is very close to the density of thermostating by deterministic scattering. The density of the Nosé–Hoover thermostat

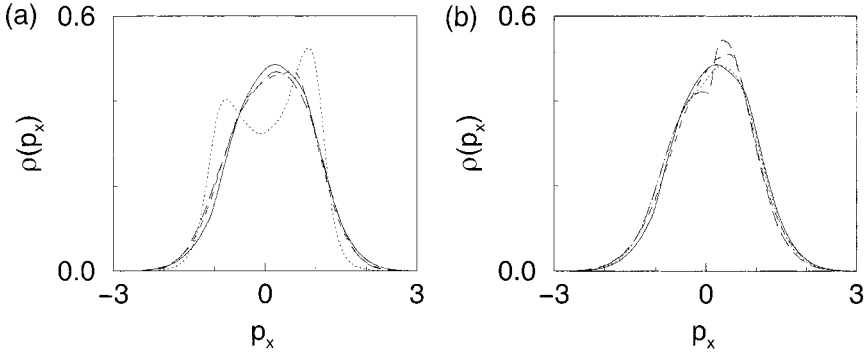

Fig. 2. Probability density $\varrho(p_x)$ for $\varepsilon = 0.5$: (a) Nosé–Hoover thermostat with $\tau^2 = 0.01$ (dotted curve), $\tau^2 = 1$ (dashed curve), $\tau^2 = 1000$ (long dashed curve) and thermostating by deterministic scattering (solid curve), (b) Nosé–Hoover thermostat with field-dependent coupling to the reservoir with $\tau^2 = 1$ (dotted curve), additional control of $\langle p^4 \rangle$ with $\tau^2 = 1$ (dashed curve), control of $\langle p_x^2 \rangle$ and $\langle p_y^2 \rangle$ separately with $\tau_x^2 = 0.1$ and $\tau_y^2 = 1000$ (long dashed curve) and thermostating by deterministic scattering (solid curve).

with separate control of p_x^2 and p_y^2 looks like a superposition of the densities of the Nosé–Hoover thermostat for small and for large τ.

In all the models the mean value of $\varrho(p_x)$ is positive, indicating a current parallel to the field direction.

5.2. Conductivity

The conductivity $\sigma = \langle p_x \rangle / \varepsilon$ for the Nosé–Hoover thermostat is shown in Fig. 3. For $\tau^2 = 0.01$ the curve is very similar to the conductivity of the Gaussian thermostated Lorentz gas.[23] For $\tau^2 = 1000$ the curve is more stretched along the ε axis and it is not clear whether it is globally decreasing or increasing. In contrast the conductivity as obtained from thermostating by deterministic scattering[27, 28] is a globally decreasing function. According to the Einstein relation, in the limit $\varepsilon \to 0$ σ should

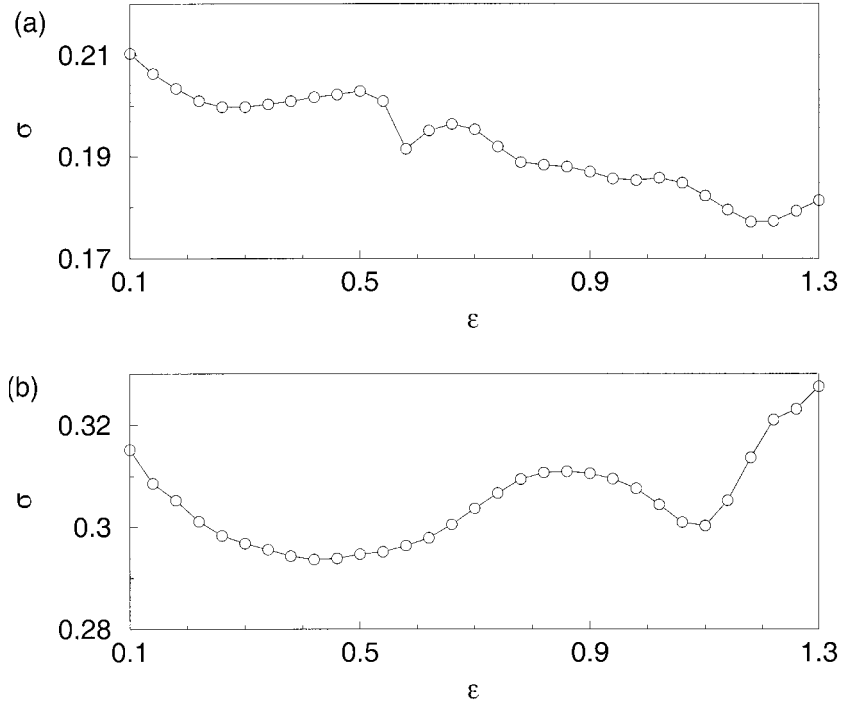

Fig. 3. Conductivity σ for the Nosé–Hoover thermostat, (a) $\tau^2 = 0.01$, (b) $\tau^2 = 1000$. The numerical uncertainty of each point is less then symbol size. For field strengths $\varepsilon < 0.1$ reliable numerical values could not be obtained $\tau^2 = 1$.

approach the equilibrium diffusion coefficient D of the periodic Lorentz gas, which for $w = 0.2361$ has the value $D \approx 0.21$.[24] This is hard to see for $\tau^2 = 1000$, because for $\varepsilon \to 0$ the probability density changes drastically from a smooth, canonical like density to a non-smooth density. It is also difficult to see any linear response in computer simulations, as has already been discussed for the Gaussian thermostated Lorentz gas and for thermostating by deterministic scattering in ref. 28.

5.3. Attractor

Figure 4 shows the Poincaré section at the moment of the collision defined by the variables $(\beta, \sin(\gamma))$, see Fig. 1b, for the Nosé–Hoover

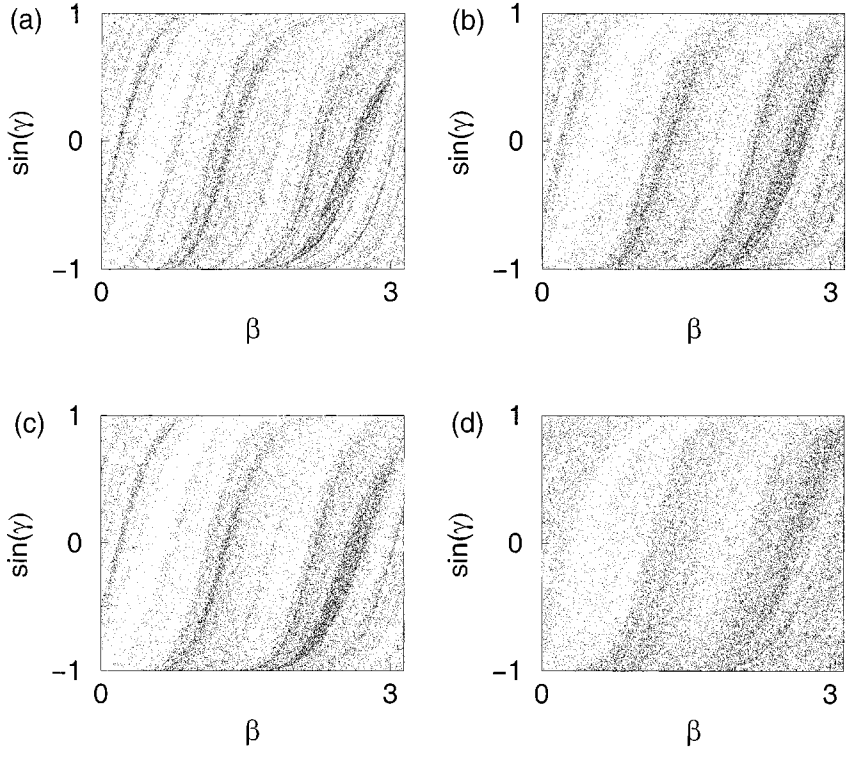

Fig. 4. Poincaré section of $(\beta, \sin\gamma)$, as defined in Fig. 1 at the moment of the collision for $\varepsilon = 1$: (a) Nosé–Hoover thermostat, $\tau^2 = 0.01$, (b)–(d) variations of the Nosé–Hoover thermostat: (b) field-dependent coupling to the reservoir, $\tau^2 = 1$, (c) additional control of p^4, $\tau^2 = 1$, (d) control of p_x^2 and p_y^2 separately, $\tau_x^2 = 0.1$ and $\tau_y^2 = 1000$.

thermostat and for the three variations. We have chosen $\varepsilon = 1.0$ and $T = 0.7740645$ to compare the results with thermostating by deterministic scattering. For all models the structure of the attractor is qualitatively the same as the structure of the attractor obtained for the Gaussian thermostated Lorentz gas[10, 11] and for the Lorentz gas as thermostated by deterministic scattering.[27, 28] The additional degree of freedom in the second and third variation does not lead to significant changes. However, the fine structure varies with the models and with the response time τ: For the Nosé–Hoover thermostat with $\tau^2 = 0.01$, see Fig. 4a, the structure is most pronounced, whereas for the control of p_x^2 and p_y^2 separately, see Fig. 4d, the structure is least visible. More results for attractors are contained in ref. 39. We remark that in refs. 11 and 24 a multifractal spectrum of dimensions has been found for the attractor of the Gaussian thermostated Lorentz gas. Because of their completely analogous structure, we expect that the attractors of our models are also multifractal.[13] More qualitative evidence, from the field dependence of the Poincaré sections, is presented below.

5.4. Bifurcation Diagram

In Figs. 5 and 6 we present the observed values of the angle β, see Fig. 1b, in the steady state over the field strength ε at the moment of the collision. These diagrams thus correspond to a reduced view of the phase space of Fig. 4 by projecting out the variable $\sin(\gamma)$. The fine structure of Fig. 4 is therefore suppressed in the following figures which emphasize the field-strength-dependence of the attractor.

Figures 5a and 5b show the bifurcation diagram for the Nosé–Hoover thermostat. For the two values of τ^2 the attractor covers the whole β interval for small field strengths $\varepsilon < 1.3$ and contracts onto a periodic orbit with increasing field strength. For $\tau^2 = 0.01$ the scenario is similar to the one of the Gaussian thermostated Lorentz gas.[23] [6] For $\tau^2 = 1000$ the scenario is complicated too, but it is less rich between these two values.[39]

In contrast to the Nosé–Hoover thermostat, the attractor of thermostating by deterministic scattering remains β interval filling even for large ε.[27, 28]

The bifurcation diagram in the dissipative limit $\tau \to \infty$ of Eqs. (1) with a constant friction coefficient ζ_c shows an inverse scenario to Figs. 5a and 5b, as is presented in Fig. 5c. For small ε the trajectory is a so-called creeping orbit,[30] then it changes to a periodic orbit, and for large ε the

[6] In Fig. 10 of ref. 23 the angle of flight after a collision is plotted and the field is parallel to the negative x-axis.

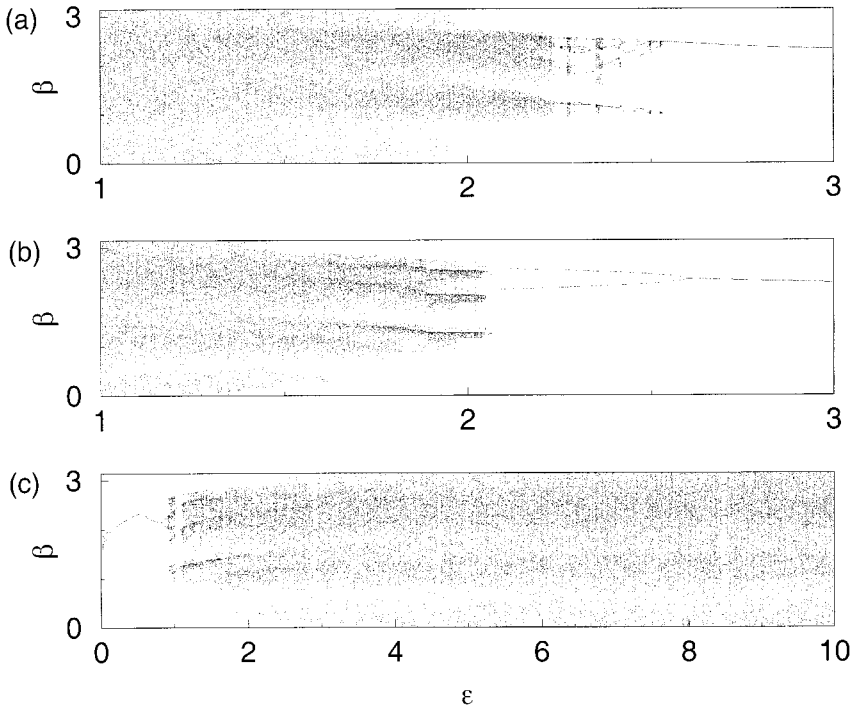

Fig. 5. Bifurcation diagram for the Nosé–Hoover thermostat, (a) $\tau^2 = 0.01$, (b) $\tau^2 = 1000$, and (c) dissipative limit, $\zeta_c = 1.0$.

attractor gets β-interval filling. By increasing ζ_c the strength of the dissipation increases with the consequence that the onset of chaotic behavior starts at higher field strengths.[39] We remark that related to the different shapes of the attractors by varying ζ_c in the dissipative limit, the duration of the transient behavior of the Nosé–Hoover thermostat grows drastically for $\tau \to \infty$.

Figure 6 shows the bifurcation diagrams for the three variations of the Nosé–Hoover thermostat. In general one observes that even for high field strengths chaotic regions appear, in contrast to the Nosé–Hoover thermostat.

For the variation with the additional control of p^4 in Fig. 6b the attractor covers a bounded β interval for $\varepsilon \geqslant 3$. For these field strengths the trajectory is a creeping orbit.

Figure 6c depicts the attractor for the variation with separate control of p_x^2 and p_y^2 under different response times for the x and y direction. Since the field acts in the x direction we have chosen a strong couplings $\tau_x^2 = 0.1$,

for the x direction and a weak coupling, $\tau_y^2 = 1000$, for the y direction. Up to a field strength $\varepsilon \approx 6.5$ no periodic window has been found. The bifurcation diagram for these parameters most strongly deviates from the Nosé–Hoover and Gaussian thermostated Lorentz gas and is closest to the bifurcation diagram of thermostating by deterministic scattering. However, in contrast to thermostating by deterministic scattering the attractor is more concentrated around $\beta \simeq \pi$.

We detected a numerical problem for the second and the third variation at several values of τ. One observes that sporadically after large time intervals there appears a creeping orbit with a very low velocity of the particle, which is difficult to handle numerically. Whether this creeping orbit is the stationary state could perhaps be clarified by calculating Lyapunov exponents.[24]

The bifurcation diagrams for the Nosé–Hoover thermostat and the three variations show a rich dynamics composed of chaotic region, chaos-order

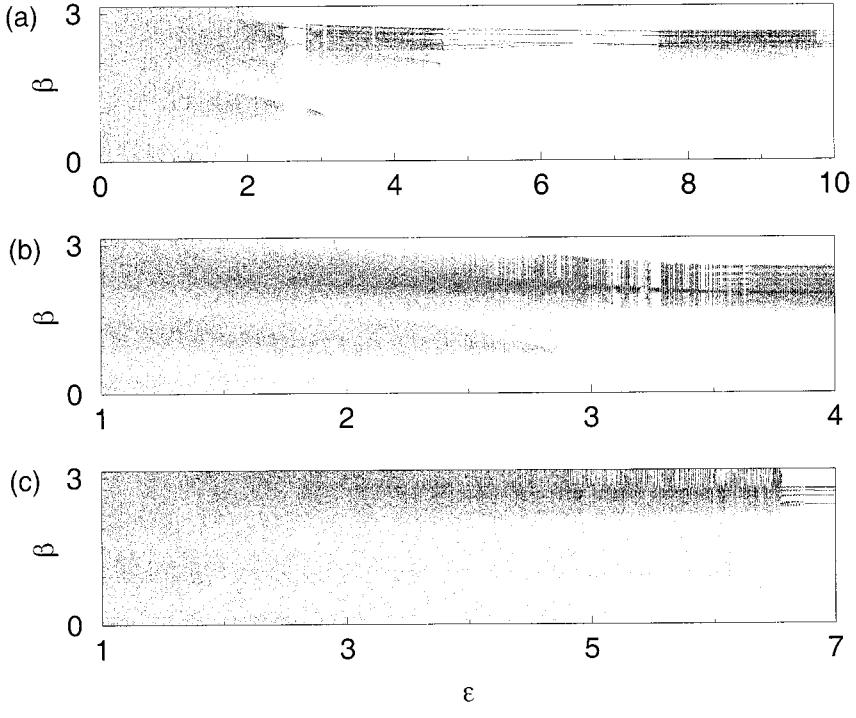

Fig. 6. Bifurcation diagram for the variations of the Nosé–Hoover thermostat: (a) field-dependent coupling to the reservoir, $\tau^2 = 1$, (b) additional control of p^4, $\tau^2 = 1$, and (c) control of p_x^2 and p_y^2 separately, $\tau_x^2 = 0.1$, $\tau_y^2 = 1000$.

transitions and periodic orbits. It would be interesting to study the field dependence of the attractor in more detail, e.g., according to which scenario does the transitions from order to chaos occur, is the dynamics nonergodic for certain parameters as it has been found for the Gaussian thermostated Lorentz gas[22] and where are the chaotic and the integrable regions.

5.5. Thermodynamic Entropy Production and Phase-Space Volume Contraction

A characteristic property of the Nosé–Hoover thermostat as well as of the Gaussian isokinetic thermostat is that the thermodynamic entropy production is equal to the phase-space volume contraction rate if one associates T to the relevant temperature.[9, 17–19] This equality can also easily be obtained for the variation with the additional control of p^4 and for the variation with separate control of p_x^2 and p_y^2.

On the other hand it does not hold for the Nosé–Hoover thermostat with field-dependent coupling to the reservoir. From Eqs. (2) one gets for the phase-space contraction rate of this model $-\langle \operatorname{div} \dot{\Gamma} \rangle = (2+\varepsilon_x)\langle \zeta \rangle$ where $\dot{\Gamma} = (\dot{\vec{q}}, \dot{\vec{p}}, \dot{\zeta})$. The precise relation between thermodynamic entropy productions $\dot{S}_{TD} = \varepsilon_x \langle p_x \rangle / T$ and $-\langle \operatorname{div} \dot{\Gamma} \rangle$ for this variation is obtained by calculating the energy balance between subsystem and reservoir:[17]

$$E = \frac{p^2}{2} + T\tau^2\zeta^2 \tag{6}$$

is the total energy the time derivative of which in a nonequilibrium steady state on average is zero,

$$\left\langle \frac{dE}{dt} \right\rangle = 0 \tag{7}$$

Inserting Eqs. (2) in Eqs. (7) leads to

$$\frac{\varepsilon_x \langle p_x \rangle}{T} = \frac{\varepsilon_x \langle p_x^2 \zeta \rangle}{T} + 2\langle \zeta \rangle \tag{8}$$

Numerical simulations have shown that p_x^2 and ζ are not independent quantities in nonequilibrium. If p_x^2 and ζ were independent and equipartition were fulfilled, $\langle p_x^2 \rangle = T$, which is only the case in equilibrium, then Eq. (8) would lead to an identity between thermodynamic entropy production and phase-space volume contraction. The results for $-\langle \operatorname{div} \dot{\Gamma} \rangle$ and for $\dot{S}_{TD}$ as obtained from computer simulations for this system are

Table I. Phase-Space Volume Contraction Rate and Thermodynamic Entropy Production for the Nosé–Hoover Thermostat with Field Dependent Coupling to the Reservoir. The Numerical Error Is $\leqslant 0.001$

	$\tau^2 = 1$		$\tau^2 = 1000$	
ε	$-\langle \operatorname{div} \dot{\Gamma} \rangle$	$\dot{S}_{TD}$	$-\langle \operatorname{div} \dot{\Gamma} \rangle$	$\dot{S}_{TD}$
0.5	0.152	0.145	0.145	0.147
1.0	0.547	0.561	0.567	0.592
1.5	1.240	1.366	1.256	1.391

presented in Table I at different τ and ε. More details of the entropy production in this variation and in a Gaussian thermostat with the same property are discussed in ref. 38.

6. CONCLUSIONS

We have investigated the Nosé–Hoover thermostat and three variations of it for the periodic Lorentz gas. All models are time-reversible and lead to well defined nonequilibrium steady states with a constant average kinetic energy of the moving particle.

The dynamical properties of these models have been compared with the Gaussian thermostated Lorentz gas and with the Lorentz gas as thermostated by deterministic scattering. The main results are the following:

1. It has been confirmed that in nonequilibrium all our models contract onto attractors similar to the multifractal attractor of the Gaussian thermostated Lorentz gas. This appears to be a typical characteristic of deterministic and time-reversible thermostating mechanisms. It would be interesting to have a mathematical proof for this statement.

2. The structure of the bifurcation diagram, the conductivity and the momentum probability densities depend on the thermostating mechanism. Concerning these properties the standard Nosé–Hoover thermostat in the periodic Lorentz gas is closer to the Gaussian thermostat than to thermostating by deterministic scattering. This is surprising, because the Nosé–Hoover thermostat and thermostating by deterministic scattering share the property of keeping the energy of the particle on average constant in nonequilibrium. In contrast, the equilibrium properties and the bifurcation diagram in nonequilibrium of the third variation are qualitatively closest to the properties of thermostating by deterministic scattering.

3. The identity between phase-space contraction and thermodynamic entropy production does not hold for the first variation. This property was accepted up to now as a general characterization of nonequilibrium steady states generated by Gaussian and Nosé-Hoover thermostats.

In summary, the existence of a multifractal attractor in nonequilibrium steady states is the only typical feature of these thermostat models. This fractal character reflects the extreme rarity, relative to *equilibrium states*, of *nonequilibrium states*. To look for additional common properties of all deterministic and time-reversible thermostats remains an important question, which is intimately related to obtaining a general characterization of nonequilibrium steady states. A more detailed investigation would emphasize quantitative comparisons of these thermostating mechanisms, including computing Lyapunov exponents and a selection of fractal dimensions.

ACKNOWLEDGMENTS

We dedicate this article to G. Nicolis, a champion of chaoticity, on occasion of his 60th birthday. K.R. and R.K. thank G. Nicolis for his continuous support and for the possibility to collaborate with him on problems of thermostating. This work has been started during the workshop "Nonequilibrium Statistical Mechanics" (Vienna, February 1999). The authors thank the organizers G. Gallavotti, H. Spohn and H. Posch for the invitation to this meeting. K.R. thanks the European Commission for a TMR grant under contract no. ERBFMBICT96-1193. R.K. acknowledges as well financial support from the European Commission and thanks H. van Beijeren for suggestions of improvements of the manuscript. W. G. Hoover appreciates the kind support of the United States Department of Energy at the Livermore Laboratory, through University of California Contract W-7405-Eng-48.

REFERENCES

1. D. J. Evans and G. P. Morriss, *Statistical Mechanics of Nonequilibrium Liquids* (Academic Press, London, 1990).
2. W. G. Hoover, *Computational Statistical Mechanics* (Elsevier, Amsterdam, 1991).
3. G. P. Morriss and C. P. Dettmann, *Chaos* **8**:321 (1998).
4. S. Nosé, *J. Chem. Phys.* **81**:511 (1984).
5. W. G. Hoover, *Phys. Rev. A* **31**:1695 (1985).
6. W. G. Hoover, A. J. C. Ladd, and B. Moran, *Phys. Rev. Lett.* **48**:1818 (1982).
7. D. J. Evans, *J. Chem. Phys.* **78**:3297 (1983).
8. D. J. Evans *et al.*, *Phys. Rev. A* **28**:1016 (1983).
9. B. L. Holian, W. G. Hoover, and H. A. Posch, *Phys. Rev. Lett.* **59**:10 (1987).

10. B. Moran and W. G. Hoover, *J. Stat. Phys.* **48**:709 (1987).
11. W. G. Hoover and B. Moran, *Phys. Rev. A* **40**:5319 (1989).
12. G. P. Morriss, *Phys. Lett. A* **134**:307 (1989).
13. W. G. Hoover, *Time Reversibility*, *Computer Simulation*, *and Chaos* (World Scientific, Singapore, 1999).
14. Microscopic simulations of complex hydrodynamic phenomena, in *NATO ASI Series B: Physics*, Vol. 292, M. Mareschal and B. L. Holian, eds. (Plenum Press, New York, 1992).
15. Chaos and irreversibility, in *Chaos*, Vol. 8, T. Tél, P. Gaspard, and G. Nicolis, eds. (American Institute of Physics, College Park, 1998).
16. N. I. Chernov and J. L. Lebowitz, *Phys. Rev. Lett.* **75**:2831 (1995).
17. H. A. Posch and W. G. Hoover, *Phys. Rev. A* **38**:473 (1988).
18. N. L. Chernov, C. L. Eyink, J. L. Lebowitz, and Y. G. Sinai, *Phys. Rev. Lett.* **70**:2209 (1993).
19. N. L. Chernov, C. L. Eyink, J. L. Lebowitz, and Y. G. Sinai, *Comm. Math. Phys.* **154**:569 (1993).
20. D. J. Evans, E. G. D. Cohen, and G. P. Morris, *Phys. Rev. A* **42**:5990 (1990).
21. H. van Beijeren and J. R. Dorfman, *Physica A* **279**:21 (2000).
22. J. Lloyd, L. Rondoni, and G. P. Morriss, *Phys. Rev. E* **50**:3416 (1994).
23. J. Lloyd, M. Niemeyer, L. Rondoni, and G. P. Morriss, *Chaos* **5**:536 (1995).
24. C. Dellago, L. Glatz, and H. A. Posch, *Phys. Rev. E* **52**:4817 (1995).
25. C. P. Dettmann and G. P. Morriss, *Phys. Rev. E* **54**:4782 (1996).
26. M. Kac, *Scientific American* **211**:92 (1964).
27. R. Klages, K. Rateitschak, and G. Nicolis, *Phys. Rev. Lett.* **84**:4268 (2000).
28. K. Rateitschak, R. Klages, and G. Nicolis, *J. Stat. Phys.* **99:**1339 (2000).
29. C. Wagner, R. Klages, and G. Nicolis, *Phys. Rev. E* **60**:1401 (1999).
30. W. G. Hoover and B. Moran, *Chaos* **2**:599 (1992).
31. W. G. Hoover, *Phys. Rev.* **40**:2814 (1989).
32. W. G. Hoover and B. L. Holian, *Phys. Lett.* **211:**253 (1996).
33. W. G. Hoover and O. Kum, *Phys. Rev. E* **56**:5517 (1997).
34. J. Jellinek and R. S. Berry, *Phys. Rev. A* **38**:3069 (1988).
35. A. Bulgac and D. Kusnezov, *Phys. Rev. A* **42**:5045 (1990).
36. G. J. Martyna, M. L. Klein, and M. Tuckerman, *J. Chem. Phys.* **97**:2635 (1992).
37. C. P. Dettmann and G. P. Morriss, *Phys. Rev. E* **55**:3693 (1997).
38. R. Klages and K. Rateitschak, unpublished.
39. K. Rateitschak, R. Klages, and W. G. Hoover, chao-dyn/9912018.